# GSA DATA REPOSITORY 2015262

*Ault et al., 2015*

## ANALYTICAL METHODS

### (U-Th)/He methods

He degassing and U-Th analyses of hematite and apatite were conducted at the University of Arizona Radiogenic Helium Dating Laboratory (ARHDL).

***Hematite***: Chips of hematite ~1-2 mm in diameter were extracted the fault surfaces using fine point tweezers and a dremel tool. These chips where then broken into replicate aliquots. Aliquots of hematite were selected to avoid dremel tool marks and minimize host-rock phases including quartz and feldspar. Aliquots contain a principle slip surface and were selected from the interior of the hematite fault coatings, greater than one $\alpha$-stopping distance (i.e., >20 $\mu$m) away from the hematite-host rock interface, so an $\alpha$-ejection correction factor is not applied to the He dates. Individual aliquots were loaded into Nb packets.

Hematite aliquots were heated to temperatures of 1000-1100 °C for 10-15 minutes using a Nd-YAG laser in an ultra-high vacuum gas extraction line. Extracted He gas was spiked with $^{3}$He, purified using cryogenic and gettering methods, and analyzed on a quadrupole mass spectrometer. Each aliquot was heated a second time to temperatures slightly greater than the first extraction but negligible gas was released. Analysis of a known quantity of $^{4}$He was performed after every 4-5 unknown analyses to monitor instrumental sensitivity drift. U and Th contents of each aliquot were measured by isotope dilution and solution ICPMS, as described by Reiners (2005). Prior analyses in the ARHDL indicate that hematite does not fully dissolve in nitric acid, hydrochloric acid, or aqua regia, requiring HF dissolution in a pressure digestion vessel (Parr bomb). Following addition of a $^{233}$U-$^{229}$Th spike, equilibration, and dissolution, U and Th isotopes were measured on an Element 2 ICP-MS. Fish Canyon Tuff zircon was used as a standard and analyzed by the same procedures with the batch of unknowns. No alpha-ejection corrections are required for the hematite He dates because the aliquots are part of a larger initial sample with dimensions larger than the alpha-stopping distance. Hematite dates were determined assuming that the grains were unzoned in U and Th.

Hematite He dates presented in Table DR1 do not exhibit a positive correlation between hematite He date and Th/U in any of the samples (Fig. DR6), supporting the interpretation that U volatilization as a result of extreme heating during degassing (Vasconcelos et al., 2013) is not an issue in these samples.

***Apatite:*** Single crystals of apatite were selected based on morphology, clarity, and lack of inclusions using a binocular microscope with crossed polars. Individual apatites were imaged, length and width dimensions measured on two sides, and loaded into Nb packets. Apatites were laser heated to 1065 °C for three minutes without a gas re-extract. Extracted He gas was spiked with $^{3}$He, purified using cryogenic and gettering methods, and analyzed on a quadrupole mass spectrometer. The degassed apatites were retrieved, spiked with a $^{233}$U-$^{229}$Th-$^{147}$Nd-$^{42}$Ca tracer, dissolved in $HNO_3$ at ~90 °C for 1 hour, and analyzed on an Element 2 ICP-MS. The apatite mass was computed as the dimensional mass from the apatite radius and length measurements. This dimensional mass was used to calculate the apatite U, Th, and Sm concentrations. Fragments of the Durango apatite were used as a standard. A hexagonal prism morphology was used as a reasonable approximation for the apatite alpha-ejection correction (Farley et al., 1996) and apatites are assumed to be unzoned in U, Th, and Sm.

**Apatite fission-track methods**

Apatite grains were mounted in epoxy resin, alumina and diamond polished, and spontaneous fission tracks revealed by etching with 5.5M $HNO_3$ at 20°C for 20 seconds. Samples were analyzed by applying the external detector method (Gleadow, 1981) using very low uranium, annealed muscovite mica detectors, and irradiated at the Oregon State University Triga Reactor, Corvallis, USA. The neutron fluence was monitored using European Institute for Reference Materials and Measurements (IRMM) uranium-dosed glasses IRMM 540R. After irradiation, induced tracks in the mica external detectors were revealed by etching with 48% HF for 18 minutes. Spontaneous and induced FT densities were counted using an Olympus BX61 microscope at 1250x magnification with automated Kinetek Stage system. Apatite FT lengths and Dpar values were measured using an attached drawing tube and digitizing tablet supplied by Trevor Dumitru of Stanford University calibrated against a stage micrometer. Central ages (Galbraith and Laslett, 1993), quoted with 1σ errors, were calculated using the IUGS

recommended Zeta-calibration approach of Hurford and Green (1983). An apatite IRMM 540R zeta calibration factor of 368.1±14.9 was obtained by repeated calibration against a number of internationally agreed age standards including Durango and Fish Canyon apatite according to the recommendations of Hurford (1990).

**Scanning electron microscopy and grain size analysis**

BSE images of representative hematite aliquots from each sample were acquired on a Quanta 650 FEG scanning electron microscope at Utah State University's Microscopy Core Facility. Aliquots used for (U-Th)/He analysis are consumed during the measurement process. Therefore, representative aliquots from each fault surface were mounted in epoxy for BSE imaging. In the case of WF94-17A, B, D, E, and F, aliquots used for grain size analysis were extracted from exactly the same sample locality as the dated aliquots to ensure that the same hematite texture and grain size (and thus closure temperature) were analyzed. Aliquots were mounted in epoxy in cross-sectional view, with no consistent orientation other than orthogonal to the principal slip surface. Thus the image orientation does not bias the grain size measurements. BSE imaging of polished, carbon-coated mounts was performed in low vacuum-variable pressure mode at 0.5-0.8 Torr, with 16-20 kV accelerating voltage, 65 nA current, and 8.5-11.4 mm working distance. Images were taken at various scales such that images at the smallest field of view are a component of the larger field of view. Images were annotated to show these relationships and the self-similarity of the grain size distribution in each aliquot (Fig. DR3).

BSE images at 50000x-80000x were used for grain size measurements (Fig. DR4). The goal of this exercise was to place bounds on the minimum and maximum mean grain radii for each sample and thus the temperature sensitivity of He loss of each of the samples in response to ambient cooling or rapid cooling from shear heating. The approximate mean radius of each of 10-20 individual grains in a ~1 $\mu m^2$ area was measured in each sample. In select cases, the ~1 $\mu m^2$ area was divided into two parts to contain regions where individual grains could be identified. Only those crystals for which boundaries could be reasonably identified were measured. Grain boundaries are commonly only observable in parts of the BSE images where some grains have been removed, likely during polishing, or where the sample is particularly thin. Because it is not possible to measure the mean radius in larger numbers of grains, we focus on

and report in the main text the maximum and minimum mean radii. We note the range in grain sizes determined in this way is particularly important for those samples extracted from a single fault surface: WF94-17A, B, D, E, and F.

**REFERENCES**


Farley, K.A., Wolf, L.T., and Silver, L.T., 1996, The effects of long alpha-stopping distances on (U-Th)/He ages. *Geochimica et Cosmochimica Acta* **60**, 4223-4229.

Galbraith, R.F., and Laslett, G.M., 1993, Statistical models for mixed fission track ages. *Nuclear Tracks* **21**, 459-470.

Gleadow, A.J.W., 1981, Fission-track dating methods: what are the real alternatives? *Nuclear Tracks* **5**, 3-14.

Hurford, A.J., 1990, Standardization of fission track dating calibration: Recommended by the Fission Track Working Group of the I.U.G.S. Subcommission on Geochronology. *Chemical Geology* **80**, 171-178.

Hurford, A.J., and Green, P.F., 1983, The zeta-age calibration of fission-track dating. *Isotope Geoscience* **1**, 285-317.

Reiners, P.W., 2005, Zircon (U-Th)/He thermochronometry. *Reviews in Mineralogy and Geochemistry* **58**, 151-179.

Reiners, P.W., 2009, Nonmonotonic thermal histories and contrasting kinetics of multiple thermochronometers. *Geochimica et Cosmochimica Acta* **73**, 3612-3629.

Reiners, P.W., Thomson, S.N., McPhillips, D., Donelick, R.A., and Roering, J.J., 2007, Wildfire thermochronology and the fate and transport of apatite in hillslope and fluvial environments. *Journal of Geophysical Research-Earth Surface* **112**, F04001.

Vasconcelos, P.M., Heim, J.A., Farley, K.A., Monteiro, H., and Waltenberg, K., 2013, $^{40}Ar/^{39}Ar$ and (U-Th)/He - $^{4}He/^{3}He$ geochronology of landscape evolution and channel iron deposits genesis at Lynn Peak, Western Australia. *Geochimica et Cosmochimica Acta* **117**, 283-312.

**Table DR1**. Hematite (U-Th)/He data from hematite-coated fault surfaces.

| | U (ng) | ± 1σ | Th (ng) | ± 1σ | Th/U | $^4$He (fmol) | ± 1σ | Date (Ma) | Error (Ma)[a] |
|---|---|---|---|---|---|---|---|---|---|
| **Samples with aliquots extracted from isolated localities on fault surface WF94-17** | | | | | | | | | |
| **WF94-17A**, 41.39011, -112.0231 [b]; 1488 m | | | | | | | | | |
| H1 | 4.010 | 0.061 | 3.249 | 0.055 | 0.810 | 103.28 | 0.73 | 4.01 | 0.06 |
| H2 | 2.494 | 0.038 | 2.042 | 0.032 | 0.819 | 64.03 | 0.52 | 3.99 | 0.06 |
| H3 | 1.365 | 0.021 | 1.060 | 0.019 | 0.776 | 35.68 | 0.32 | 4.10 | 0.06 |
| **WF94-17B**, 41.39011, -112.0231; 1488 m | | | | | | | | | |
| H1 | 2.150 | 0.032 | 3.331 | 0.053 | 1.549 | 40.70 | 0.36 | 2.57 | 0.04 |
| H2 | 0.579 | 0.009 | 0.935 | 0.015 | 1.616 | 10.00 | 0.19 | 2.32 | 0.05 |
| H3 | 1.477 | 0.023 | 2.175 | 0.034 | 1.472 | 28.63 | 0.29 | 2.67 | 0.04 |
| **WF94-17D**, 41.39011, -112.0231; 1488 m | | | | | | | | | |
| H1 | 0.422 | 0.006 | 0.435 | 0.006 | 1.056 | 10.34 | 0.15 | 3.65 | 0.07 |
| H2 | 0.223 | 0.003 | 0.231 | 0.003 | 1.060 | 5.84 | 0.14 | 3.90 | 0.10 |
| H3 | 0.277 | 0.004 | 0.285 | 0.004 | 1.055 | 7.29 | 0.11 | 3.93 | 0.08 |
| H4 | 0.336 | 0.005 | 0.367 | 0.005 | 1.121 | 9.05 | 0.15 | 3.97 | 0.08 |
| **WF94-17E**, 41.39011, -112.0231; 1488 m | | | | | | | | | |
| H1 | 0.608 | 0.009 | 0.856 | 0.012 | 1.445 | 12.49 | 0.14 | 2.86 | 0.05 |
| H2 | 0.423 | 0.006 | 0.640 | 0.009 | 1.552 | 9.14 | 0.14 | 2.95 | 0.05 |
| H3 | 0.218 | 0.003 | 0.364 | 0.005 | 1.718 | 5.77 | 0.14 | 3.52 | 0.09 |
| H4 | 0.096 | 0.001 | 0.221 | 0.003 | 2.357 | 2.66 | 0.13 | 3.33 | 0.17 |
| **WF94-17F**, 41.39011, -112.0231; 1488 m | | | | | | | | | |
| H1 | 1.373 | 0.020 | 0.761 | 0.011 | 0.568 | 45.43 | 0.38 | 5.43 | 0.08 |
| H2 | 1.577 | 0.023 | 0.837 | 0.012 | 0.545 | 50.29 | 0.37 | 5.26 | 0.08 |
| H3 | 1.596 | 0.023 | 1.024 | 0.015 | 0.658 | 52.55 | 0.37 | 5.30 | 0.07 |
| **Sample with aliquots extracted from multiple localities on WF94-17** | | | | | | | | | |
| **WF94-17C**, 41.39011, -112.0231; 1488 m | | | | | | | | | |
| H1 | 0.696 | 0.011 | 1.001 | 0.015 | 1.440 | 17.05 | 0.22 | 3.39 | 0.06 |
| H2 | 0.638 | 0.010 | 0.566 | 0.566 | 0.887 | 14.98 | 0.20 | 3.60 | 0.07 |
| H3 | 0.107 | 0.002 | 0.120 | 0.120 | 1.117 | 1.96 | 0.06 | 2.68 | 0.08 |
| H4 | 0.263 | 0.004 | 0.318 | 0.318 | 1.206 | 6.30 | 0.13 | 3.45 | 0.08 |
| H5 | 0.202 | 0.003 | 0.227 | 0.227 | 1.123 | 5.51 | 0.08 | 4.00 | 0.08 |
| **Samples with aliquots extracted from multiple localition on fault surface** | | | | | | | | | |
| **A13-1**, 41.3796, -112.0218; 1490 m | | | | | | | | | |
| H1 | 0.141 | 0.002 | 0.414 | 0.006 | 2.941 | 6.17 | 0.11 | 4.79 | 0.10 |
| H2 | 0.126 | 0.002 | 0.319 | 0.005 | 2.538 | 6.48 | 0.11 | 5.96 | 0.12 |
| H3 | 0.342 | 0.005 | 0.897 | 0.013 | 2.622 | 19.16 | 0.26 | 6.41 | 0.11 |
| H4 | 1.661 | 0.024 | 6.302 | 0.091 | 3.795 | 86.27 | 0.99 | 5.07 | 0.08 |
| H5 | 1.105 | 0.016 | 3.705 | 0.053 | 3.352 | 59.78 | 0.67 | 5.59 | 0.08 |
| H6 | 0.571 | 0.008 | 1.497 | 0.021 | 2.623 | 31.36 | 0.43 | 6.29 | 0.11 |
| H7 | 0.330 | 0.005 | 0.867 | 0.012 | 2.626 | 14.19 | 0.20 | 4.92 | 0.09 |
| H8 | 1.440 | 0.021 | 3.450 | 0.049 | 2.395 | 81.41 | 0.81 | 6.69 | 0.10 |
| **A13-3**, 41.3797, -112.0214; 1485 m | | | | | | | | | |
| H1 | 0.136 | 0.002 | 0.166 | 0.002 | 1.222 | 17.49 | 0.21 | 18.44 | 0.30 |
| H2 | 0.435 | 0.006 | 0.909 | 0.013 | 2.088 | 38.29 | 0.42 | 10.91 | 0.17 |
| H3 | 0.407 | 0.006 | 0.568 | 0.008 | 1.395 | 45.91 | 0.57 | 15.71 | 0.26 |
| H4 | 0.882 | 0.013 | 1.286 | 0.018 | 1.457 | 63.14 | 0.72 | 9.87 | 0.16 |
| H5 | 1.616 | 0.023 | 1.808 | 0.026 | 1.119 | 81.48 | 0.86 | 7.39 | 0.11 |
| H6 | 0.750 | 0.011 | 1.336 | 0.019 | 1.780 | 46.28 | 0.61 | 8.04 | 0.14 |

| | | | | | | | | | |
|---|---|---|---|---|---|---|---|---|---|
| H7 | 0.666 | 0.010 | 1.031 | 0.015 | 1.549 | 82.69 | 0.88 | 16.85 | 0.26 |
| H8 | 0.401 | 0.006 | 0.600 | 0.009 | 1.496 | 32.44 | 0.35 | 11.08 | 0.17 |
| **A13-5a**, 41.3795, -112.0218; 1483 m | | | | | | | | | |
| H1 | 0.289 | 0.004 | 0.630 | 0.009 | 2.183 | 12.35 | 0.22 | 5.23 | 0.11 |
| H2 | 0.146 | 0.003 | 0.466 | 0.007 | 3.196 | 7.76 | 0.19 | 5.61 | 0.15 |
| H3 | 0.024 | 0.000 | 0.064 | 0.001 | 2.703 | 0.91 | 0.06 | 4.30 | 0.29 |
| H4 | 0.032 | 0.001 | 0.082 | 0.001 | 2.517 | 1.56 | 0.07 | 5.58 | 0.26 |
| H5 | 0.054 | 0.001 | 0.167 | 0.003 | 3.111 | 1.92 | 0.07 | 3.83 | 0.15 |
| **A13-7b**, 41.3793, -112.0211; 1456 m | | | | | | | | | |
| H1 | 2.102 | 0.033 | 0.457 | 0.007 | 0.218 | 64.76 | 0.47 | 5.44 | 0.09 |
| H2 | 2.706 | 0.041 | 0.576 | 0.009 | 0.213 | 76.13 | 0.67 | 4.97 | 0.08 |
| H3 | 1.459 | 0.022 | 0.391 | 0.006 | 0.268 | 40.49 | 0.38 | 4.84 | 0.08 |
| H4 | 3.966 | 0.065 | 1.076 | 0.015 | 0.271 | 103.50 | 0.81 | 4.55 | 0.08 |
| H5 | 2.600 | 0.040 | 0.755 | 0.012 | 0.290 | 72.31 | 0.50 | 4.83 | 0.07 |

[a] 1σ propagated error from analytical uncertainties on U, Th, and He analyses.

[b] Latitude and longitude reported in decimal degrees.

**Table DR2.** Apatite (U-Th)/He data from the Farmington Canyon Complex gneiss, Wasatch Fault footwall

| | Dim. mass (mg) | r[a] (μm) | l[b] (μm) | U (ppm) | Th (ppm) | [eU] (ppm) | Sm (ppm) | $^4$He (nmol/g) | Ft[c] | Raw Date (Ma) | Corr Date (Ma) | Error[d] (Ma) |
|---|---|---|---|---|---|---|---|---|---|---|---|---|
| **A13-10**, 41.3796, -112.0217; 1489 m | | | | | | | | | | | | |
| a1 | 0.0007 | 30.3 | 95.0 | 36.988 | 18.111 | 41.244 | 118.980 | 0.330 | 0.56 | 1.48 | 2.65 | 0.14 |
| a2 | 0.0006 | 28.3 | 97.5 | 42.776 | 22.734 | 48.118 | 73.570 | 0.469 | 0.54 | 1.81 | 3.35 | 0.22 |
| a3 | 0.0005 | 30.3 | 62.0 | 36.008 | 19.129 | 40.504 | 95.589 | 0.247 | 0.51 | 1.13 | 2.19 | 0.27 |
| a4 | 0.0006 | 28.0 | 94.0 | 50.027 | 15.917 | 53.767 | 103.692 | 0.356 | 0.53 | 1.23 | 2.29 | 0.16 |
| a5 | 0.0012 | 36.0 | 117.5 | 41.574 | 21.286 | 46.576 | 107.551 | 0.389 | 0.62 | 1.54 | 2.48 | 0.09 |
| | | | | | | | | | | | ***Mean ± std. dev.: 2.6 ± 0.5 Ma*** | |
| **A13-11**, 41.3801, -112.0204; 1477 m | | | | | | | | | | | | |
| a1 | 0.0015 | 32.8 | 179.0 | 27.154 | 13.947 | 30.431 | 88.428 | 0.238 | 0.62 | 1.45 | 2.33 | 0.11 |
| a2 | 0.0013 | 31.5 | 160.0 | 22.103 | 11.093 | 24.709 | 93.915 | 0.184 | 0.60 | 1.38 | 2.28 | 0.12 |
| a3 | 0.0011 | 30.5 | 143.5 | 18.973 | 12.083 | 21.813 | 85.034 | 0.154 | 0.59 | 1.30 | 2.21 | 0.13 |
| a4 | 0.0016 | 42.5 | 109.0 | 13.803 | 5.590 | 15.117 | 62.944 | 0.105 | 0.66 | 1.29 | 1.95 | 0.13 |
| a5 | 0.0013 | 35.3 | 127.5 | 19.880 | 7.188 | 21.569 | 68.905 | 0.129 | 0.62 | 1.11 | 1.78 | 0.12 |
| a6 | 0.0012 | 33.3 | 133.0 | 23.131 | 7.988 | 25.008 | 60.621 | 0.340 | 0.61 | 2.52 | 4.13 | 0.27 |
| a7 | 0.0008 | 30.0 | 112.5 | 30.449 | 11.384 | 33.125 | 78.476 | 0.210 | 0.57 | 1.18 | 2.06 | 0.12 |
| | | | | | | | | | | | ***Mean ± std. dev.: 2.4 ± 0.8 Ma*** | |

[a] r - radius.

[b] l - length.

[c] Ft - alpha ejection correction of Farley et al., 1996.

[d] 1σ propagated error from the analytical uncertainties on U, Th, and He analyses and grain-length measurement uncertainties.

**Table DR3.** Apatite fission-track data from corresponding samples to table DR2.

| Sample No. | No. of Crystals | Track Density (x $10^6$ tr $cm^{-2}$) | | | $\rho_s/\rho_i \pm 1\sigma$ | Mean Dpar (μm) | Age Dispersion | Central Age ± 1σ (Ma) |
|---|---|---|---|---|---|---|---|---|
| | | $\rho_s$ ($N_s$) | $\rho_i$ ($N_i$) | $\rho_d$ ($N_d$) | | | ($P\chi^2$) | |
| **A13-10** | 30 | 0.05373 (25) | 1.994 (928) | 0.7959 (2547) | 0.0269±0.0056 | 1.89 | 0.01% (90.2%) | **3.95±0.82** |
| **A13-11** | 40 | 0.04982 (47) | 1.359 (1282) | 0.7891 (2525) | 0.0367±0.0057 | 1.98 | 2.75% (84.7%) | **5.32±0.83** |

Notes:

(i). Analyses by external detector method using 0.5 for the $4\pi/2\pi$ geometry correction factor;

(ii). Ages calculated using dosimeter glass: IRMM540R with $\zeta_{540R}$ = 368.1±14.9 (apatite);

(iii). $P\chi^2$ is the probability of obtaining a $\chi^2$ value for v degrees of freedom where v = no. of crystals - 1;

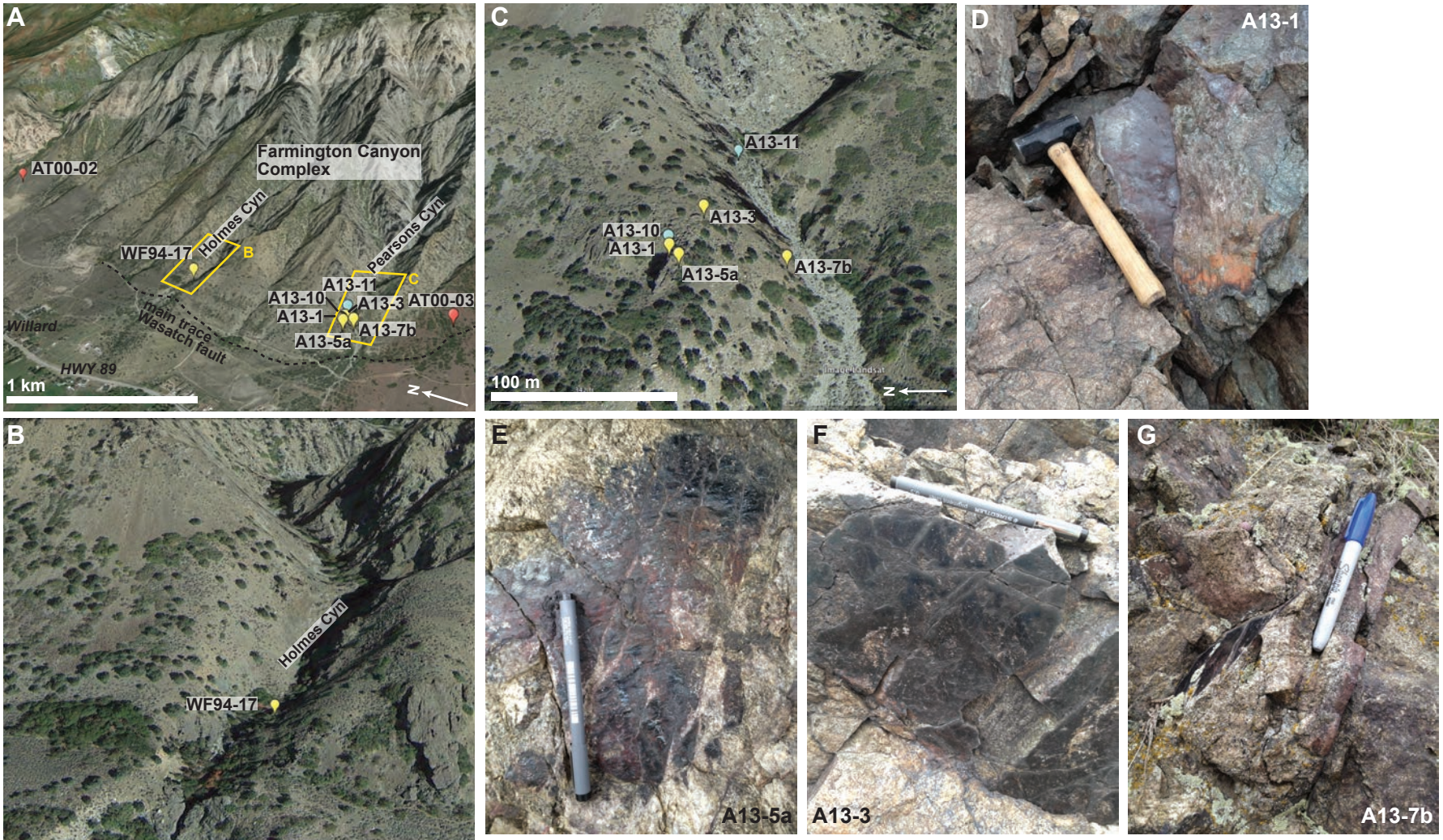


**Figure DR1. A.** Google Earth image of the study area, southern Brigham City segment of the Wasatch fault zone, showing the location of hematite fault surfaces (yellow balloons), host rock thermochronology samples (cyan balloons), and Armstrong et al. (2004) thermochronology samples (red balloons). Yellow polygons outline the regions in B and C. **B and C.** Zoom in of Holmes (B) and Pearsons (C) canyons showing sample locations. **D-G.** Field photographs of hematite-coated fault surfaces.

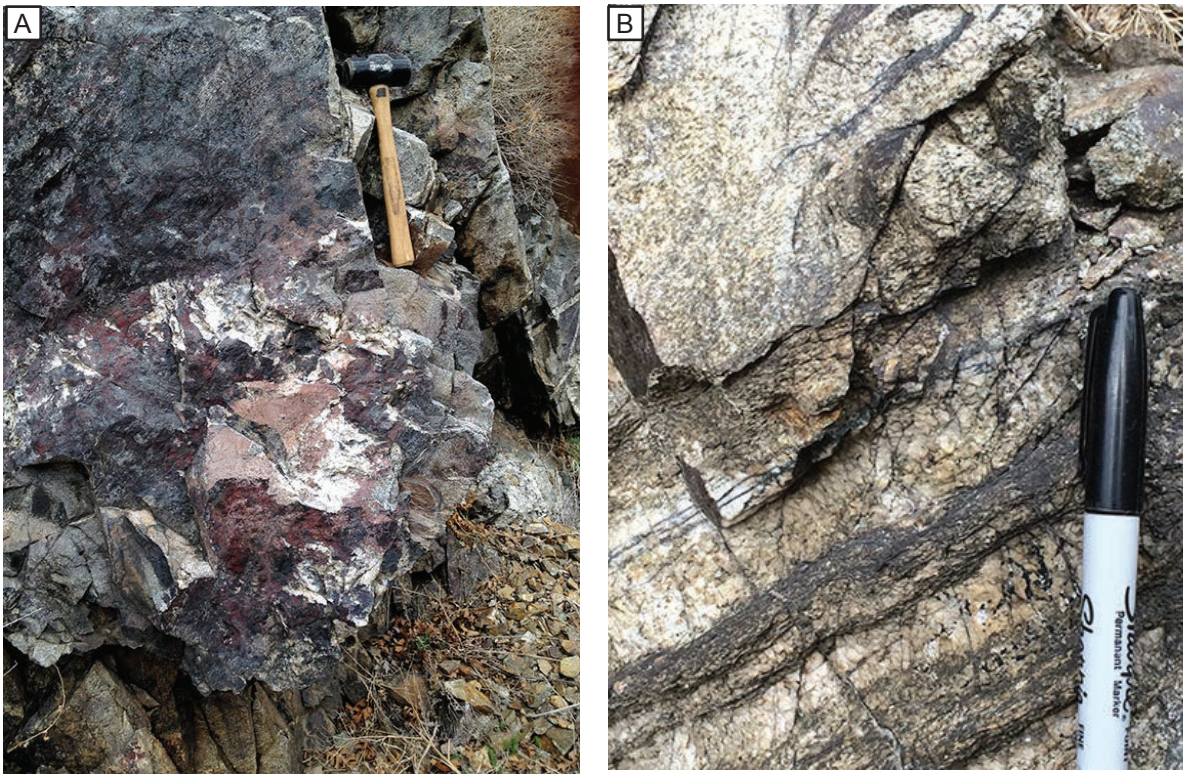


**Figure DR2. A, B:** Field photographs of specular hematite veins associated with pegmatite in the Farmington Canyon Complex.

**Figure DR3.** Hematite aliquot photomicrographs and BSE images from representative aliquots.

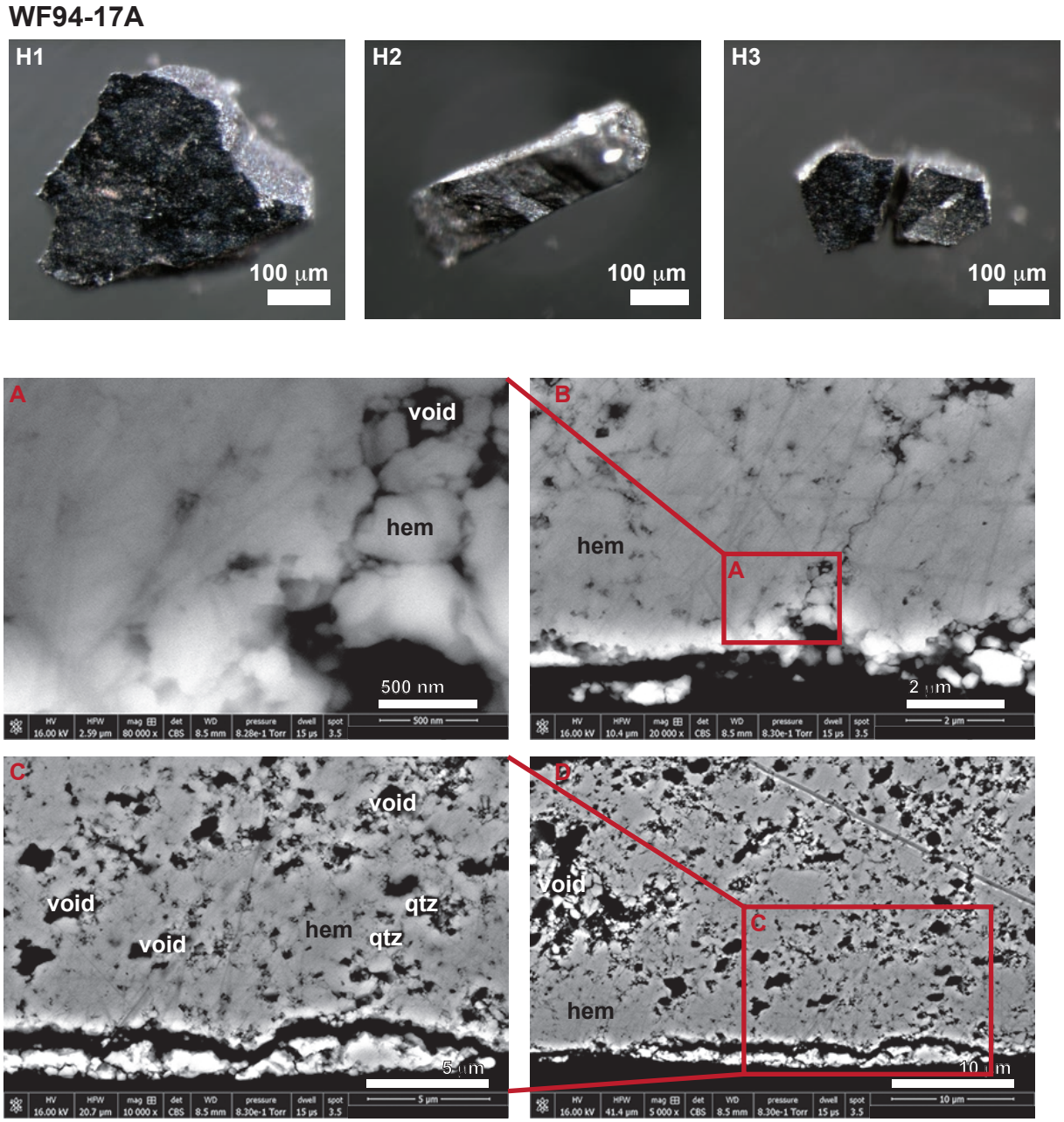

**Figure DR3 continued.** Hematite aliquot photomicrographs and BSE images from representative aliquots.

**WF94-17B**

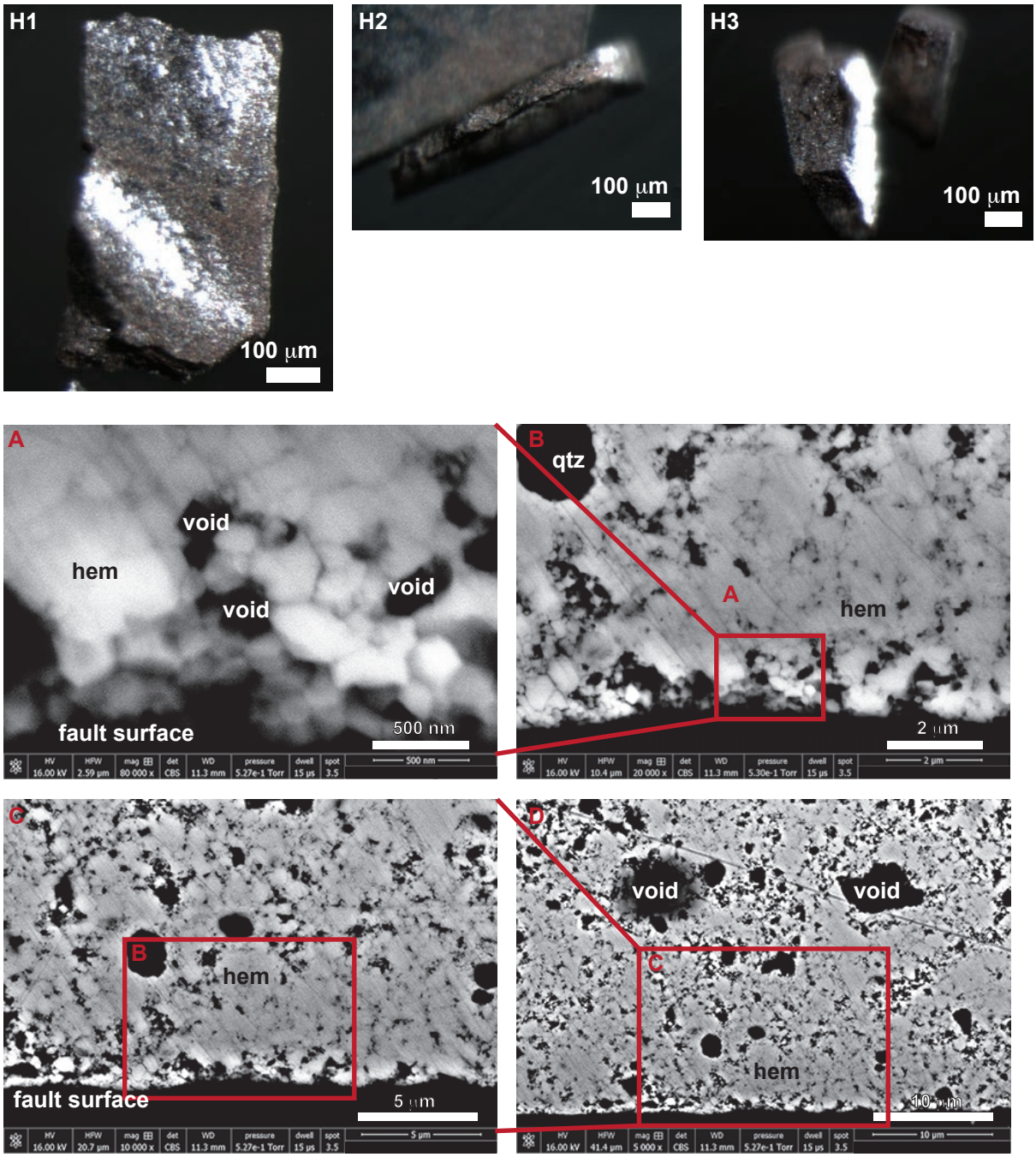

**Figure DR3 continued.** Hematite aliquot photomicrographs and BSE images from representative aliquots.

**WF94-17D**

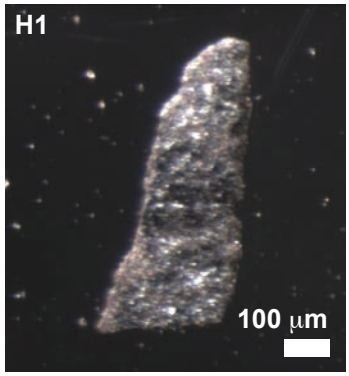


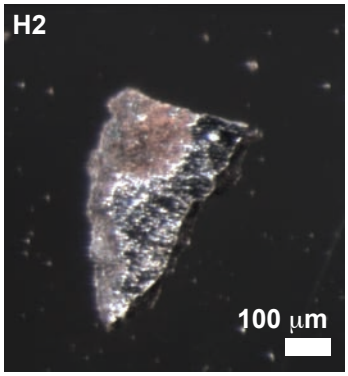


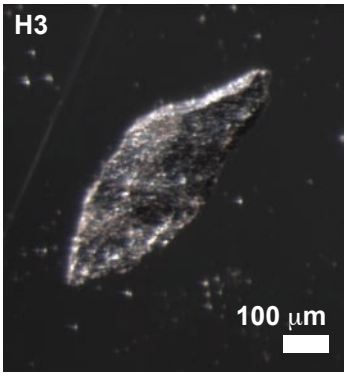


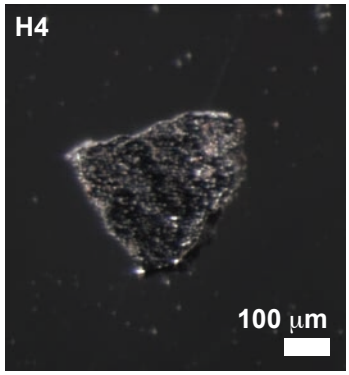


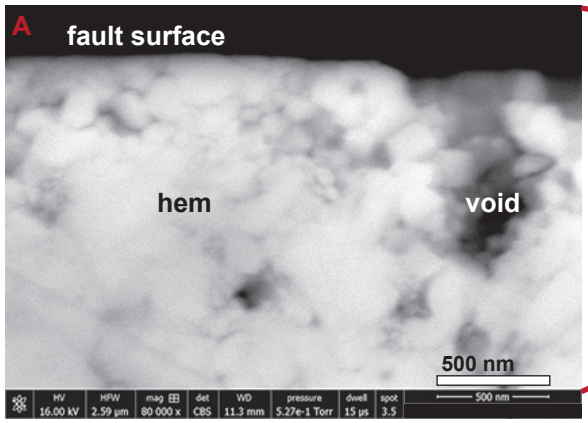


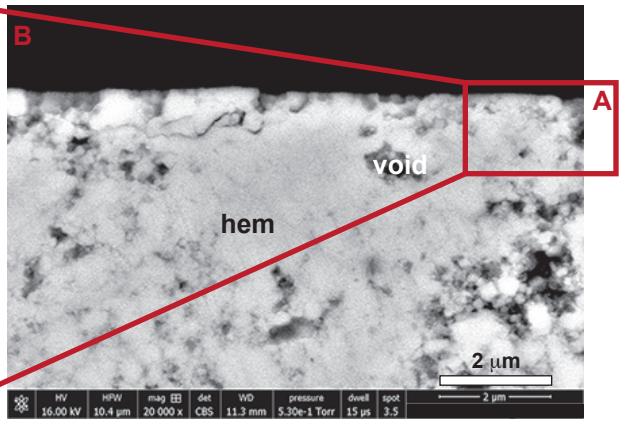


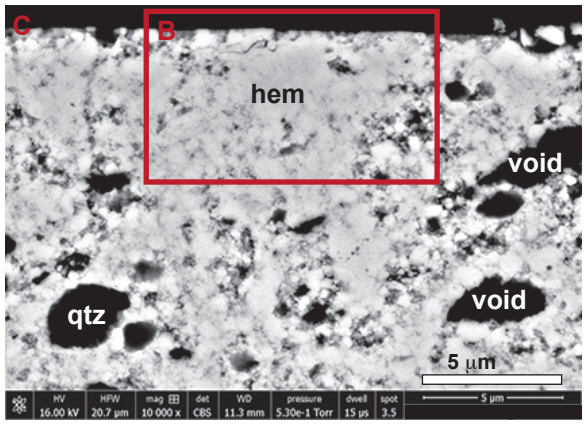

**Figure DR3 continued.** Hematite aliquot photomicrographs and BSE images from representative aliquots.

**WF94-17E**

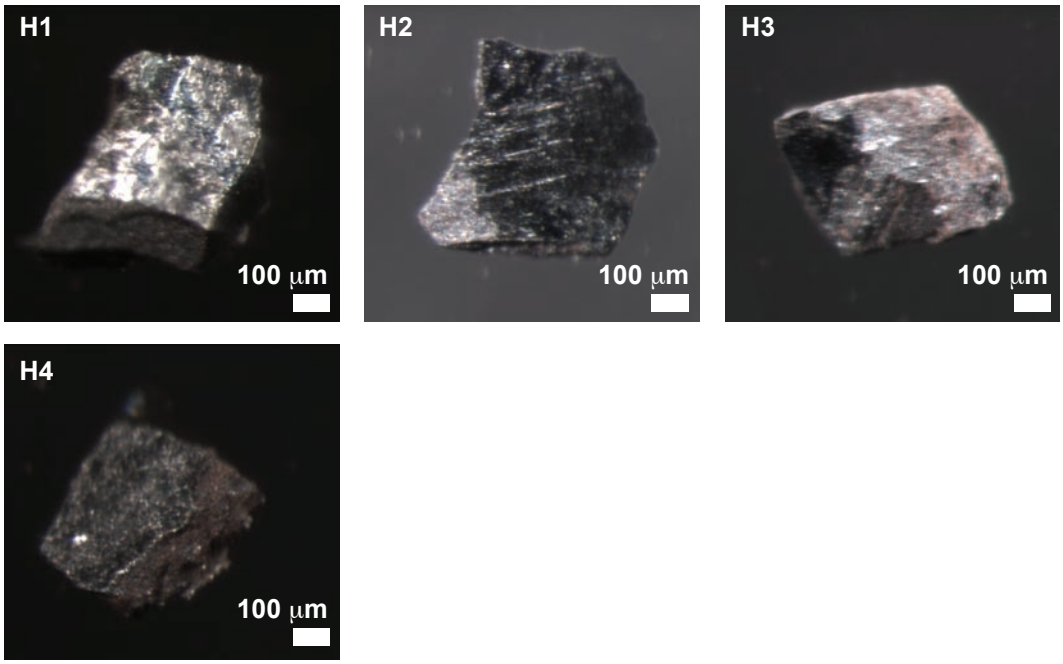


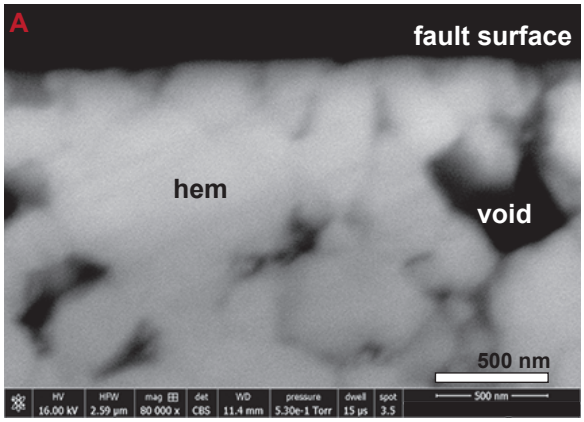


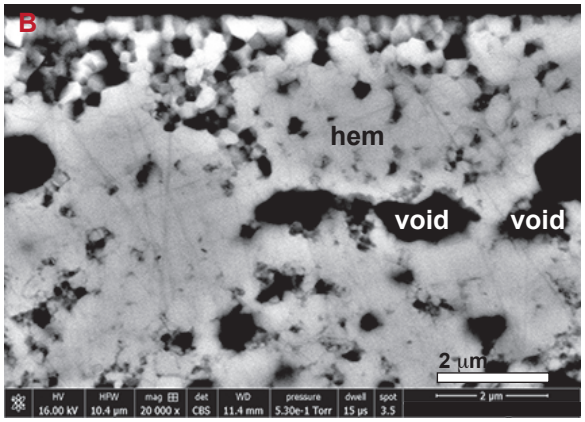


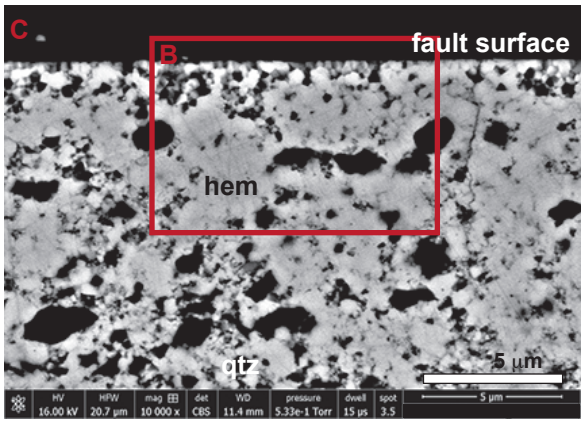

**Figure DR3 continued.** Hematite aliquot photomicrographs and BSE images from representative aliquots.

**WF94-17F**

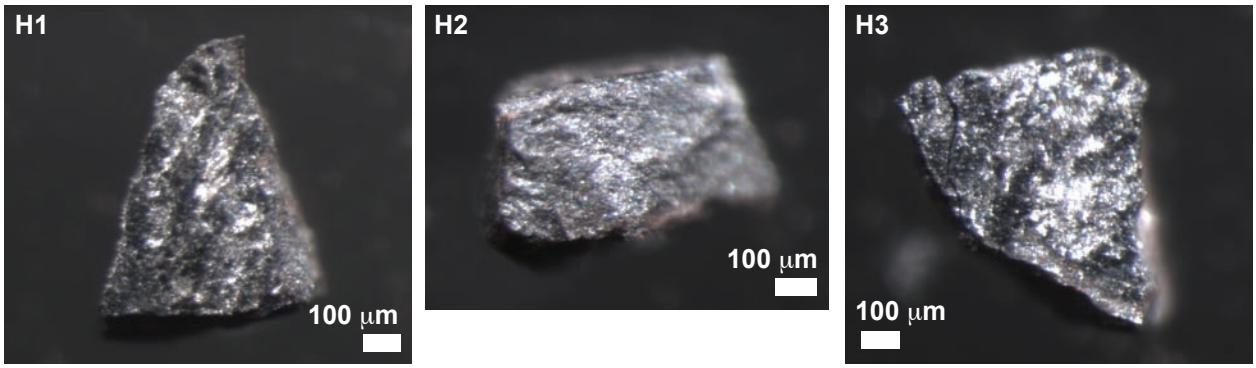


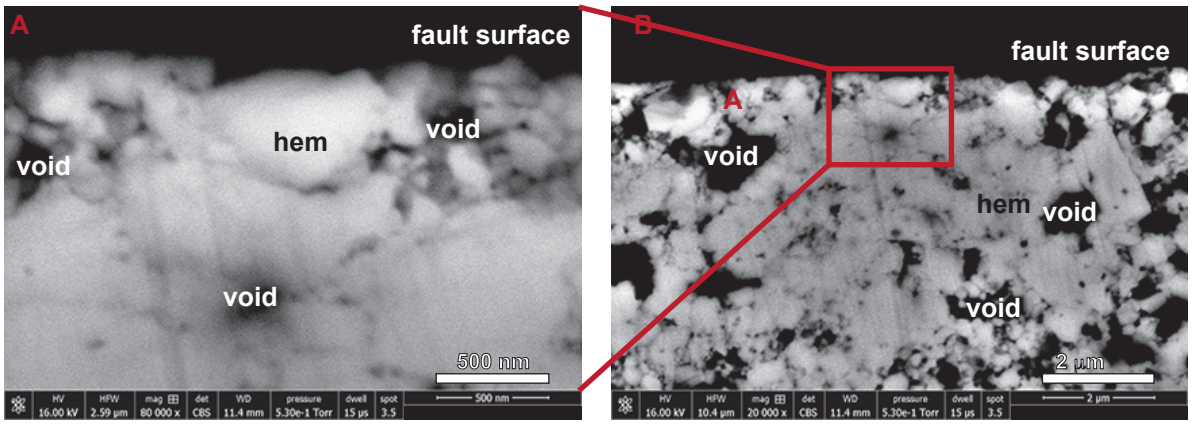


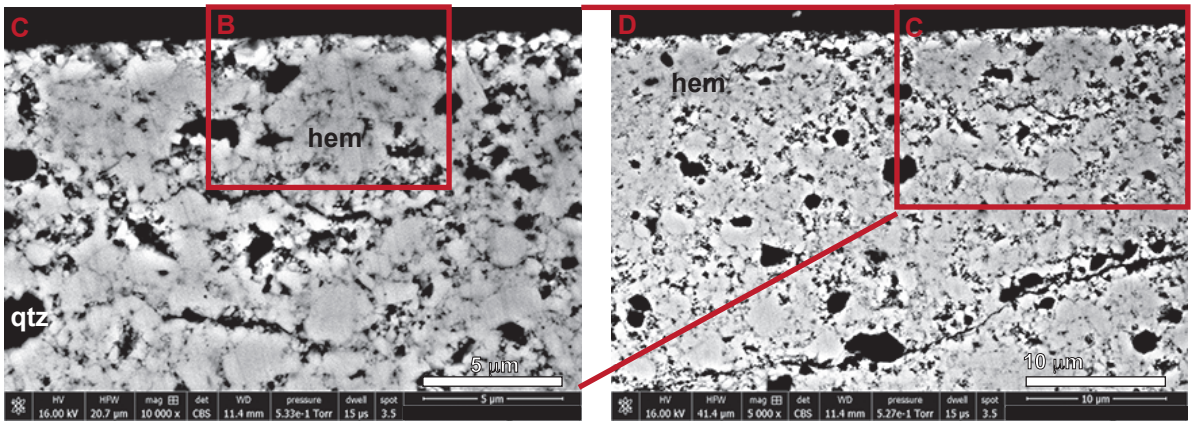

**Figure DR3 continued.** Hematite aliquot photomicrographs and BSE images from representative aliquots.

**A13-1**

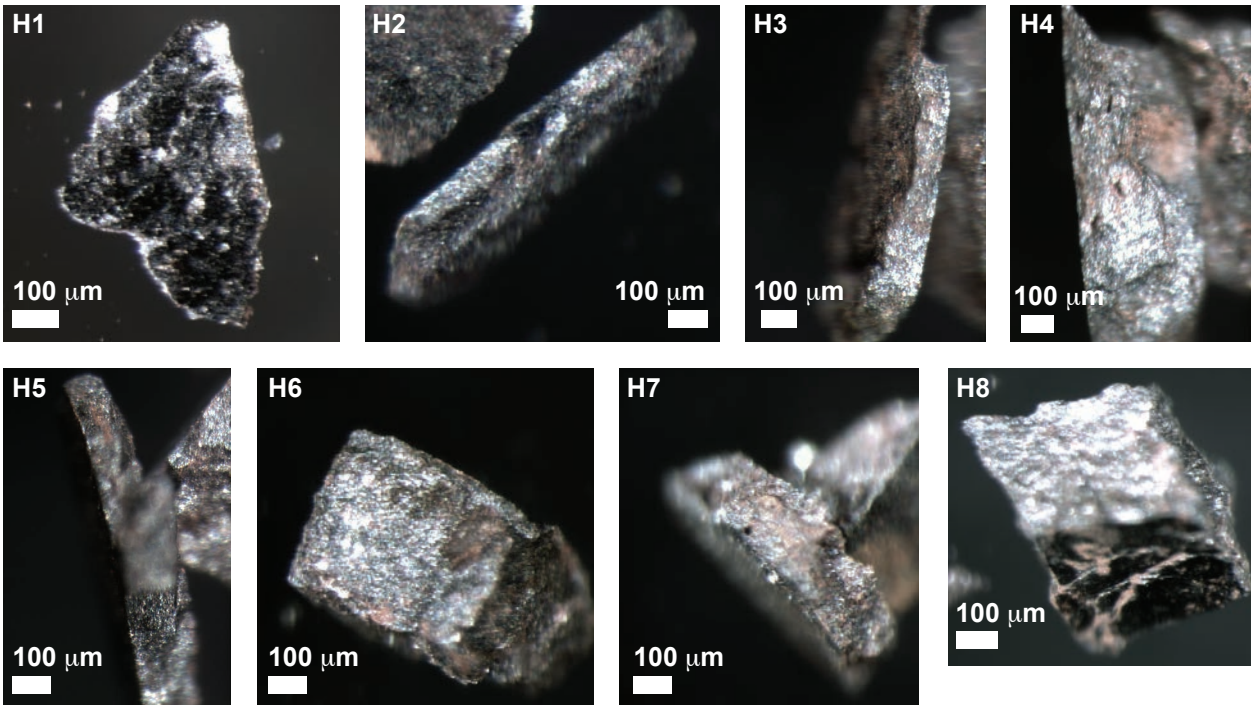


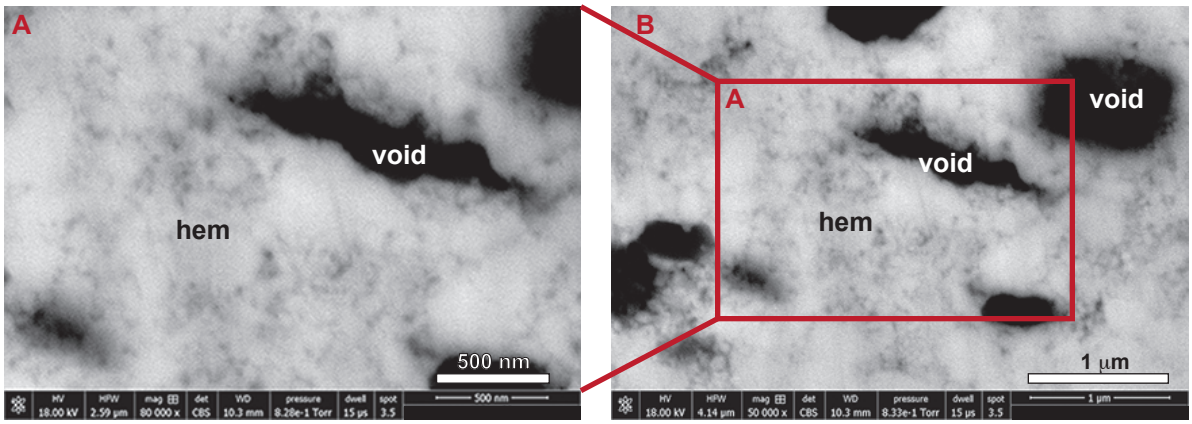


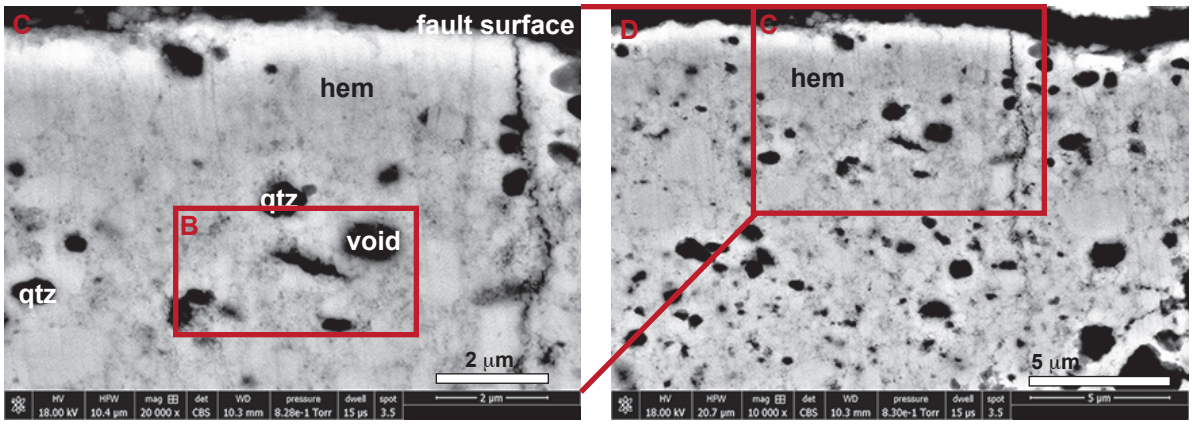

**Figure DR3 continued.** Hematite aliquot photomicrographs and BSE images from representative aliquots.

**A13-3**

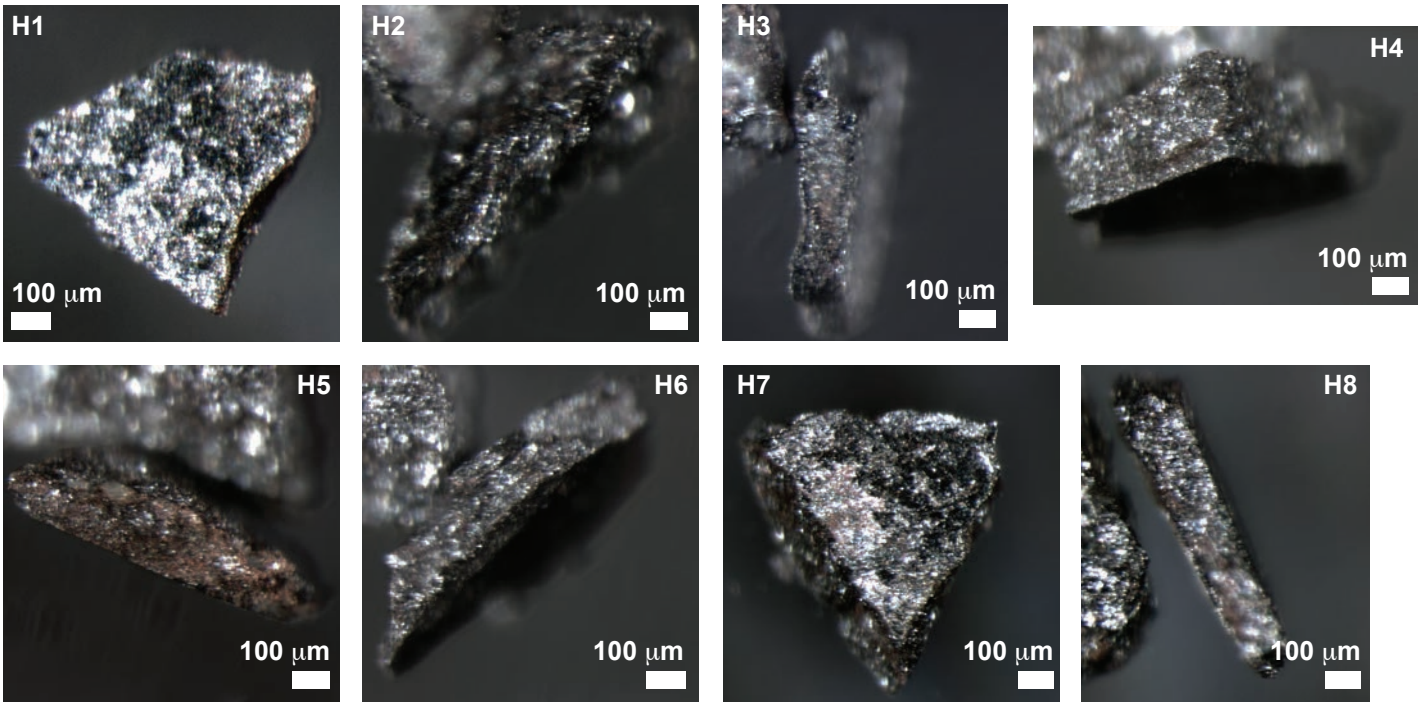


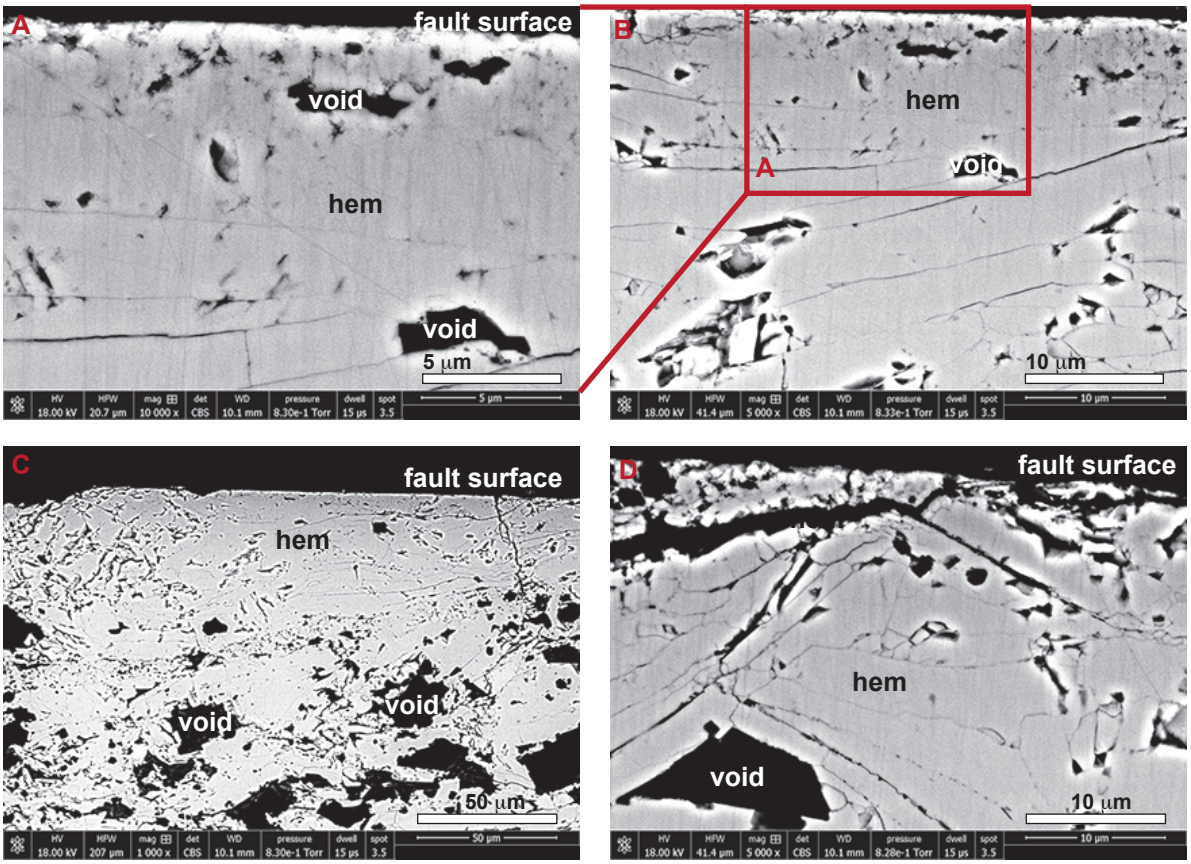

**Figure DR3 continued.** Hematite aliquot photomicrographs and BSE images from representative aliquots.

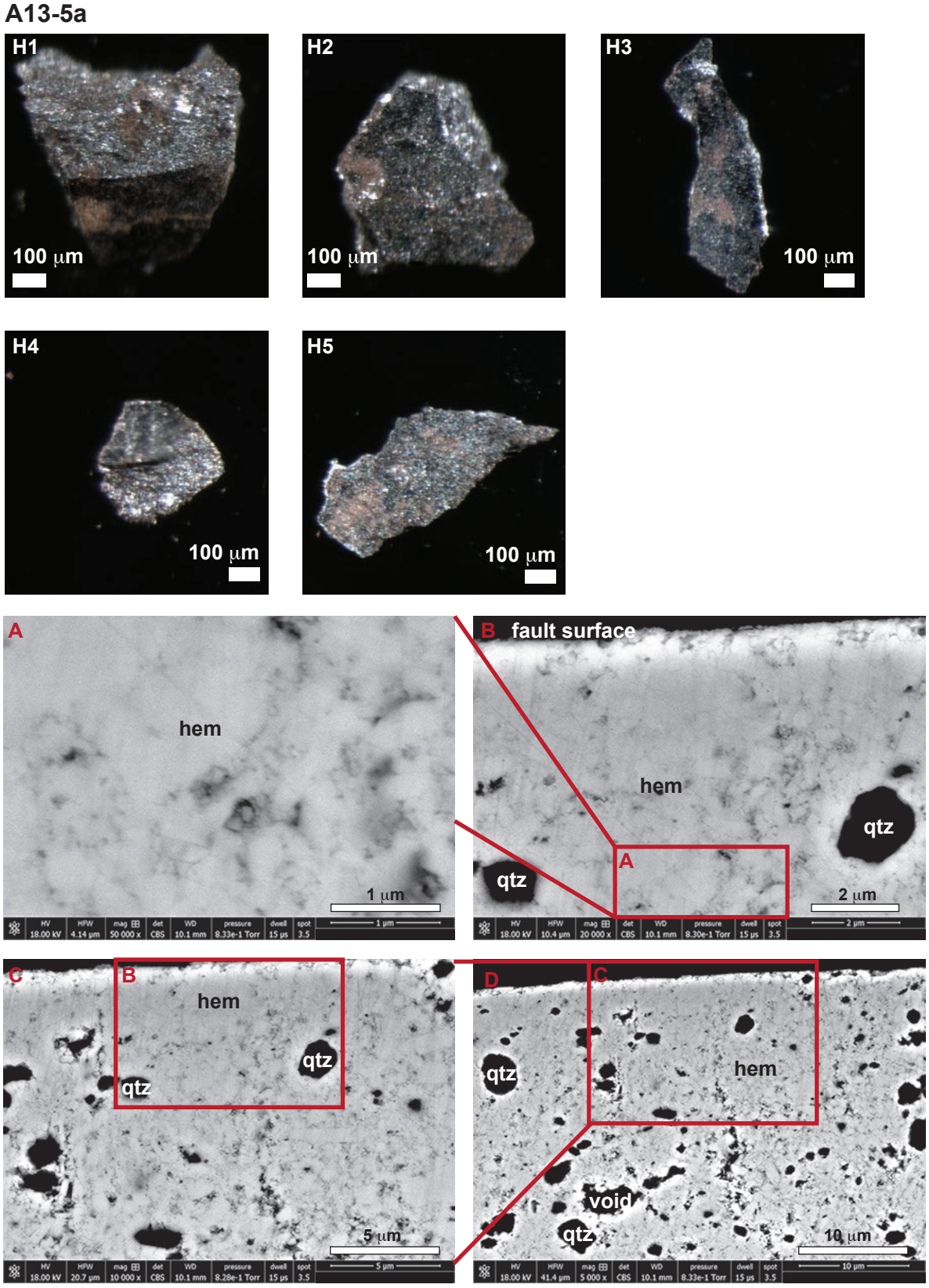

**Figure DR3 continued.** Hematite aliquot photomicrographs and BSE images from representative aliquots.

**A13-7b**

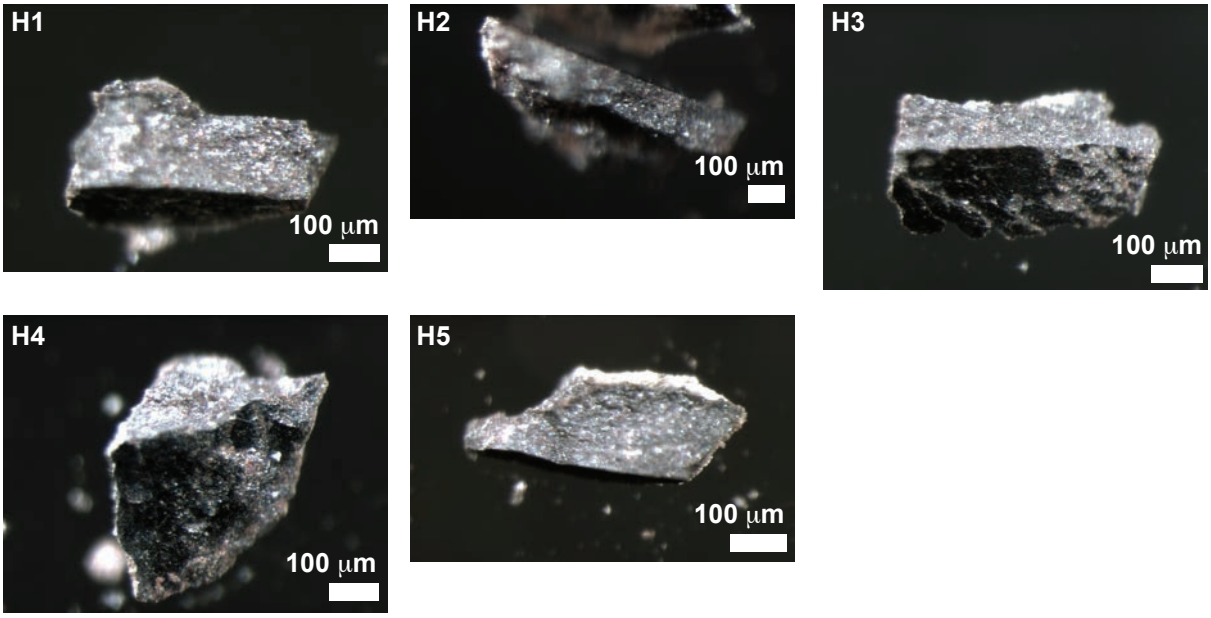


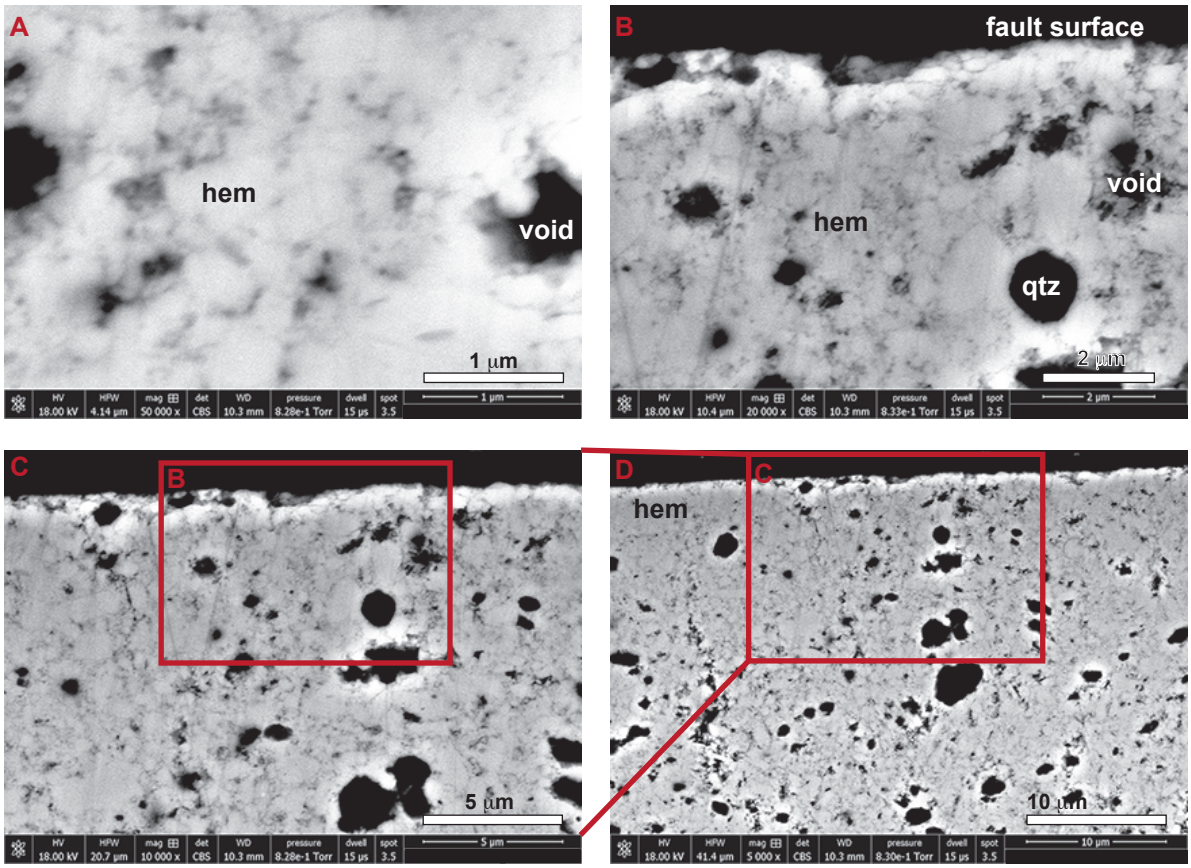

**Figure DR3 continued.** Hematite aliquot photomicrographs and BSE images from representative aliquots.

**WF94-17C**

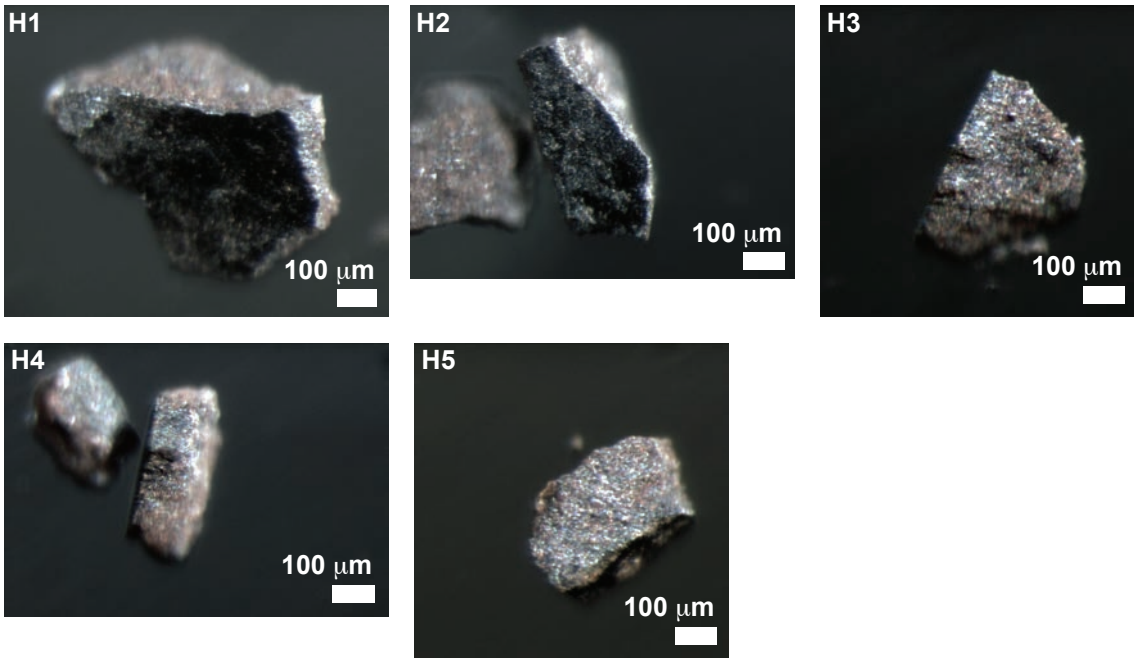


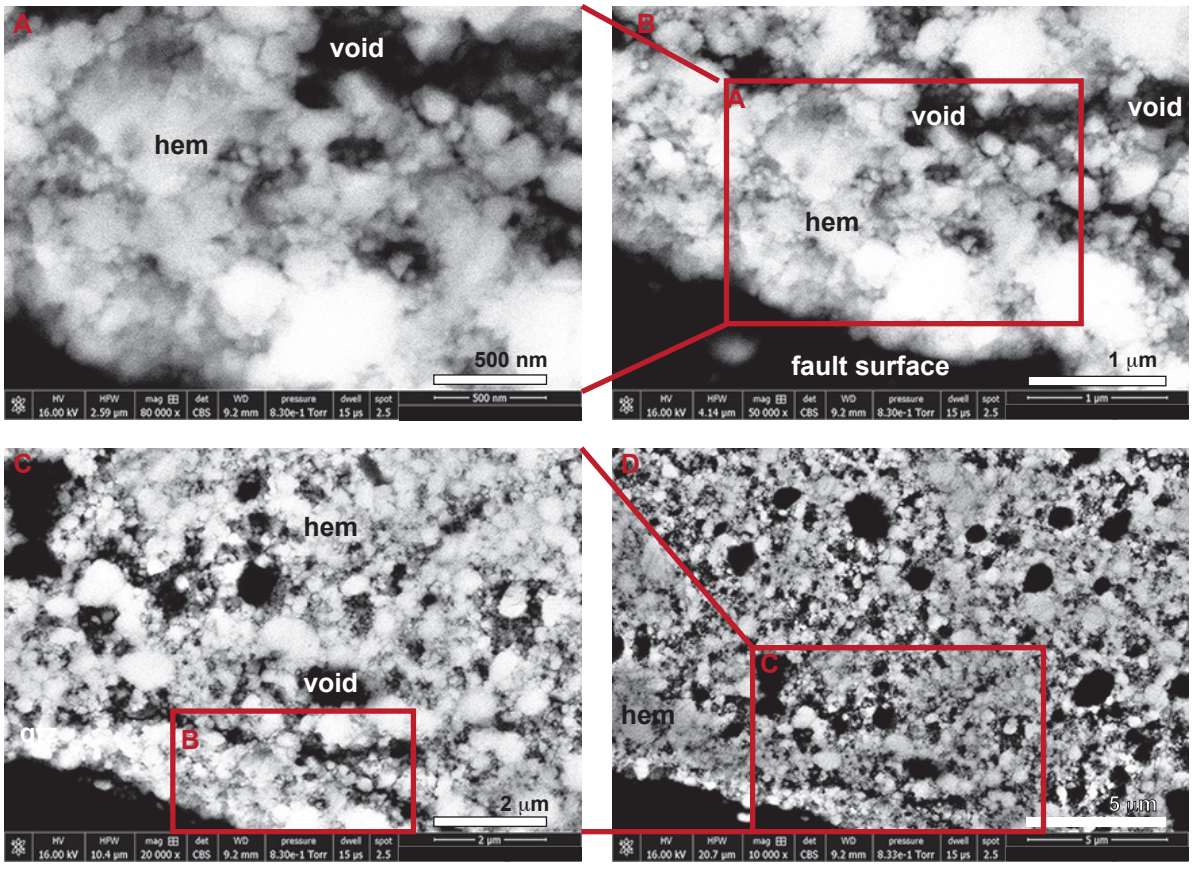

**Figure DR4.** Tracings of individual hematite grains from BSE images of representative hematite aliquots

Aliquots from isolated locations on WF94-17 fault surface

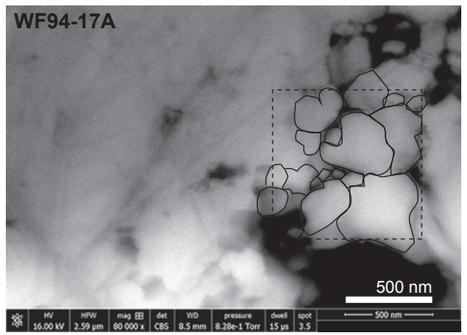


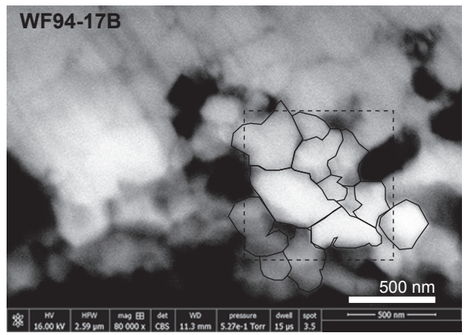


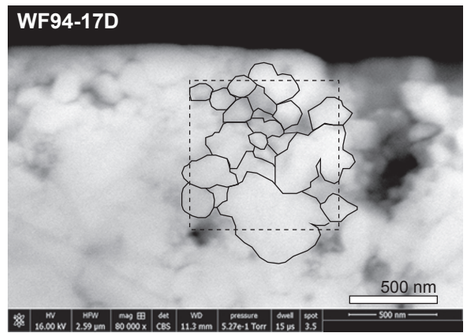


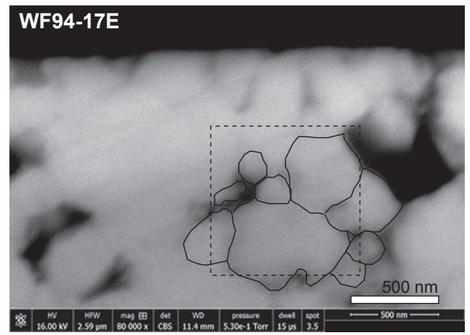


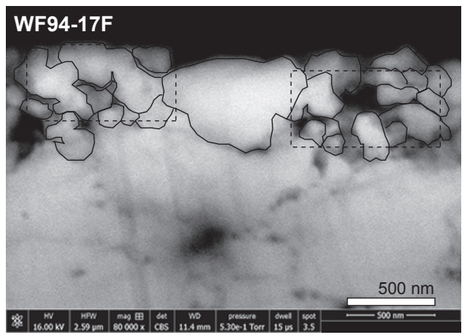


Samples with aliquots extracted from multiple locations on the same fault surface

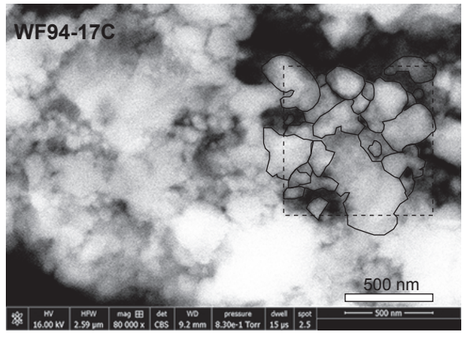


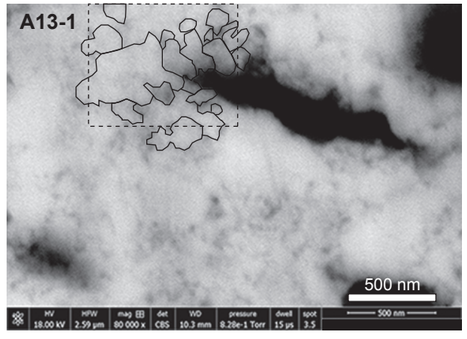


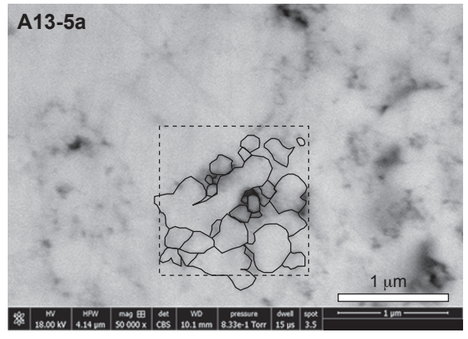


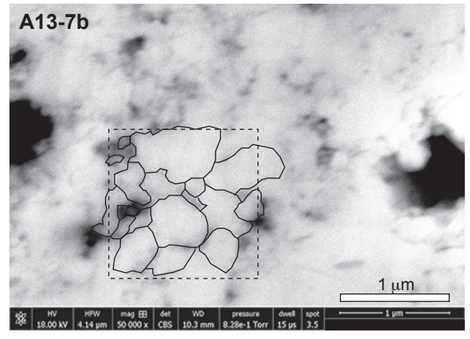


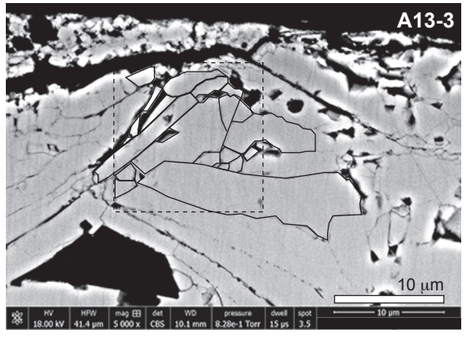

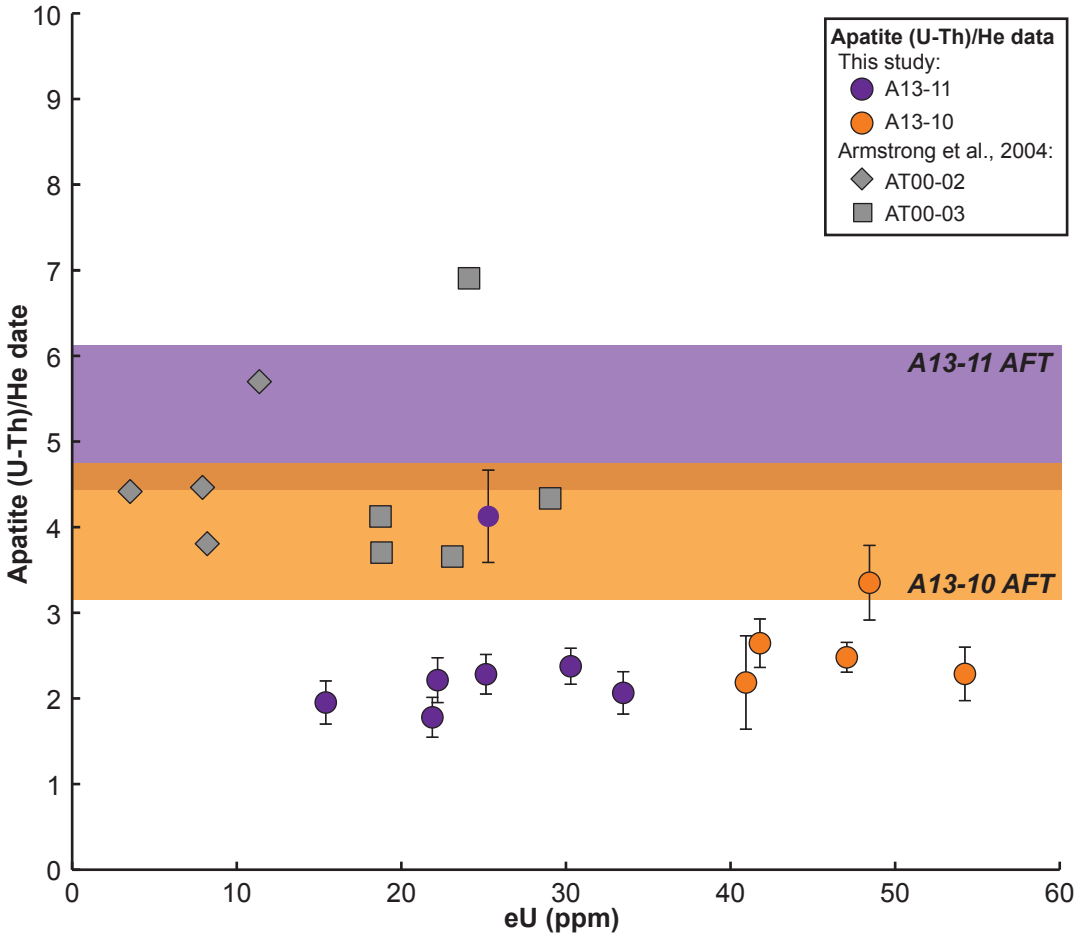


**Figure DR5:** Individual apatite (U-Th)/He date as a function of eU for two Farmington Canyon Complex gneiss samples (A13-10, A13-11). Error bars at 2σ. Shaded polygons denote the range of corresponding AFT dates (pooled age and 1σ) for these two samples. Apatite He data of Armstrong et al. (2004; AT00-02, AT00-03) also shown with gray symbols.

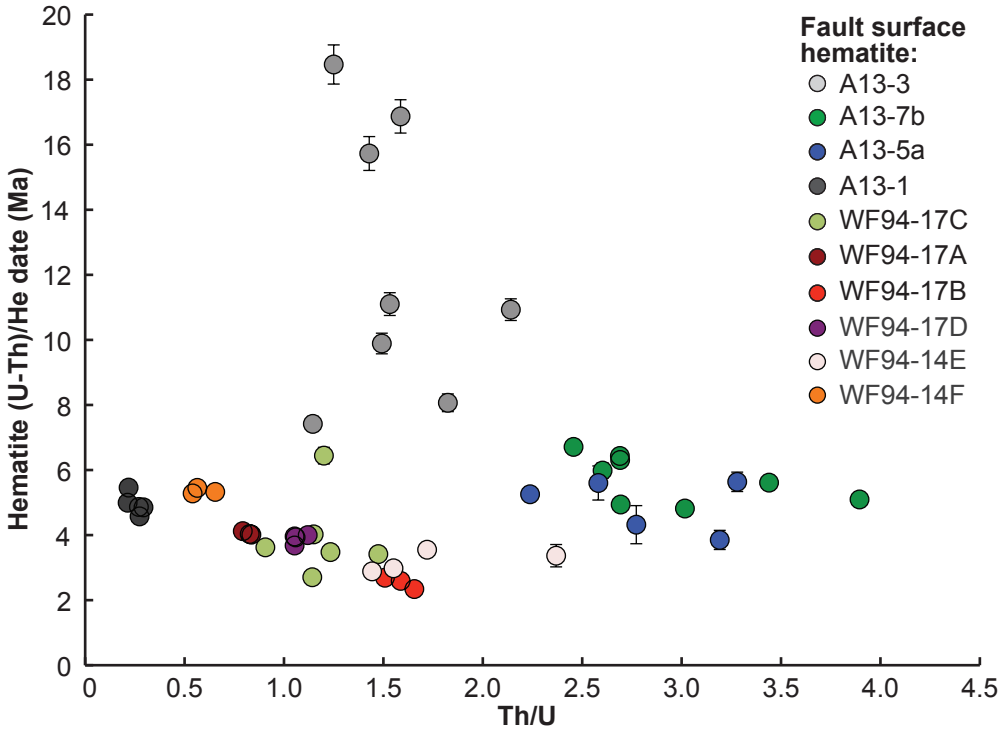


**Figure DR6.** Individual hematite (U-Th)/He date as a function of Th/U ratio. Data classified according to sample. Individual date errors plotted as the 2σ analytical uncertainity.